

# *In vivo* evaluation of a neural stem cell-seeded prosthesis

E K Purcell, J P Seymour, S Yandamuri and D R Kipke

Department of Biomedical Engineering, University of Michigan, Lurie Biomedical Engineering Building, 1101 Beal Ave., Ann Arbor, MI 48109-2099, USA

E-mail: [erinfred@umich.edu](mailto:erinfred@umich.edu) and [dkipke@umich.edu](mailto:dkipke@umich.edu)

Received 18 November 2008


Accepted for publication 10 February 2008

Published 13 March 2009

Online at [stacks.iop.org/JNE/6/026005](http://stacks.iop.org/JNE/6/026005)

## Abstract

Neural prosthetics capable of recording or stimulating neuronal activity may restore function for patients with motor and sensory deficits resulting from injury or degenerative disease. However, overcoming inconsistent recording quality and stability in chronic applications remains a significant challenge. A likely reason for this is the reactive tissue response to the devices following implantation into the brain, which is characterized by neuronal loss and glial encapsulation. We have developed a neural stem cell-seeded probe to facilitate integration of a synthetic prosthesis with the surrounding brain tissue. We fabricated parylene devices that include an open well seeded with neural stem cells encapsulated in an alginate hydrogel scaffold. Quantitative and qualitative data describing the distribution of neuronal, glial, and progenitor cells surrounding seeded and control devices are reported over four time points spanning 3 months. Neuronal loss and glial encapsulation associated with cell-seeded probes were mitigated during the initial week of implantation and exacerbated by 6 weeks post-insertion compared to control conditions. We hypothesize that graft cells secrete neuroprotective and neurotrophic factors that effect the desired healing response early in the study, with subsequent cell death and scaffold degradation accounting for a reversal of these results later. Applications of this biohybrid technology include future long-term neural recording and sensing studies.

 This article has associated online supplementary data files

(Some figures in this article are in colour only in the electronic version)

## Introduction

Neuroprosthetic devices have the capacity to record signals from a patient's uninjured cortex. These signals may then be used to place an exterior assistive device under the patient's control, thus restoring function while circumventing nervous tissue that has been damaged by injury or disease (Schwartz *et al* 2006, Donoghue *et al* 2007, Fitzsimmons *et al* 2007). In the last decade, monkeys were shown to be able to successfully control a cursor on a computer screen or a robotic arm using voluntary cortical signals (Taylor *et al* 2002, Carmena *et al* 2003). These feats have been demonstrated more recently by tetraplegic humans implanted years after injury (Hochberg *et al* 2006, Donoghue *et al* 2007). Further, cortical control of a complex, multi-jointed robotic arm with a 'hand' gripper has

been achieved by monkeys during a self-feeding task (Velliste *et al* 2008). Thus, neuroprostheses have the potential to restore some level of function to over 200 000 patients currently suffering from full or partial paralysis in the USA (Polikov *et al* 2005).

While such results are encouraging, these devices are currently plagued by inconsistent performance in terms of recording longevity and stability (Rousche and Normann 1998, Liu *et al* 1999, 2006, Williams *et al* 1999, Nicolelis *et al* 2003, Polikov *et al* 2005, Schwartz *et al* 2006). In order for neuroprostheses to be useful in research and clinical settings, stable, long-term recordings from large populations of neurons in multiple brain areas must be reliably and reproducibly achieved (Lebedev and Nicolelis 2006). Following implantation into the brain, a reactive tissue

response occurs to the prostheses, which is believed to be a major contributing factor to their inconsistent performance. An encapsulation layer composed of microglia and astrocytes isolates the device from the surrounding tissue, and neuronal density within the effective recording radius of the probe is reduced (Edell *et al* 1992, Turner *et al* 1999, Szarowski *et al* 2003, Kim *et al* 2004, Biran *et al* 2005, Polikov *et al* 2005). The glial sheath creates a diffusion barrier to the transmission of ions through the extracellular space which may affect recording quality (Roitbak and Sykova 1999). Additionally, impedance magnitude at 1 kHz (the nominal bandwidth of an action potential) increases at recording sites with 'extensive' glial reactivity (Williams *et al* 2007). While the relationship between recording quality and neuronal density has yet to be defined, it is reasonable to believe that neuronal loss would result in a reduction of signal quality. The reported 40% loss of neuronal density within 100  $\mu\text{m}$  of the device surface in the first month after implantation is particularly concerning, given that this region produces the large amplitude, reliably separated spikes useful for neural prostheses (Henze *et al* 2000, Biran *et al* 2005).

The tissue response to implanted prostheses is a characteristic reaction to central nervous system (CNS) damage (Silver and Miller 2004). Stem and progenitor cell therapy have shown promise as one approach to repair CNS injury, where the cause of recovery may be cell replacement and reinnervation. Alternatively, the 'bystander' or 'chaperone' effect, which describes the ability of transplanted cells to support host tissue by secreting therapeutic factors, correcting a biochemical deficit or inhibiting cytotoxic injury processes, may be the mechanism of healing (Teng *et al* 2002, Lindvall *et al* 2004, Pluchino *et al* 2005, Gaillard *et al* 2007). In support of the bystander effect, several studies suggest that undifferentiated neural stem cells (NSCs) have an innate ability to promote healing and axonal regeneration of host neurons as well as a reduction in glial scar formation (Ourednik *et al* 2002, Teng *et al* 2002, Lu *et al* 2003, Heine *et al* 2004, Llado *et al* 2004, Pluchino *et al* 2005). This is believed to be due to constitutive secretion of multiple neurotrophic factors (Ourednik *et al* 2002, Teng *et al* 2002, Lu *et al* 2003, Llado *et al* 2004), as well as degrading molecules which are inhibitory to axonal growth (Heine *et al* 2004). Additionally, the ability of neural precursor cells to protect injured CNS tissue by maintaining an undifferentiated state and displaying neuroprotective immune functions has been reported (Pluchino *et al* 2005).

In recent years, reports of seeding synthetic materials with cells to improve the integration of implanted devices with living tissue have emerged (Stieglitz 2007). This 'biohybrid' approach has been used to intervene in the foreign body response to implanted devices in a variety of experimental paradigms. Vascular endothelial growth factor-secreting cells have been used to induce angiogenesis surrounding implantable glucose sensors and improve their function (Klueh *et al* 2005). Coating biosensor materials with adipose-derived stromal cells has been explored as a means of reducing fibrous capsule formation around prostheses (Prichard *et al* 2007, 2008). Seeding cochlear implants with brain-derived

neurotrophic factor (BDNF)-secreting fibroblasts enhanced the survival of neighboring spiral ganglion neurons (Rejali *et al* 2007). Limited studies which describe biohybrid neural prostheses and their *in vivo* assessment exist. Kennedy reports the use of a segment of sciatic nerve placed inside a cone electrode to encourage axonal growth into the electrode (Kennedy 1989). Recordings were taken over 200 days in rats, and a later study revealed central myelinated axons and dendrites penetrating the device (Kennedy *et al* 1992). The 'sieve electrode' is designed to potentially contain embryonic neurons to restore the interface between lesioned peripheral nerves and muscle (Stieglitz *et al* 2002). To our knowledge, no reports of *in vivo* evaluations of cell-seeded cortical neural prostheses are currently available.

In this study, we developed an NSC-seeded biohybrid probe hypothesized to improve device integration with brain tissue, and evaluated the tissue response to the probes *in vivo* in rats over a 3 month time period. These parylene probes contain a hollow well containing an NSC-seeded alginate hydrogel scaffold. Alginate is a biocompatible polysaccharide polymer which forms a hydrogel following cross-linking with divalent cations such as calcium. This material is commonly used to encapsulate secretory cells, localize them to an implant site, and provide an immuno-isolating barrier between the engrafted cells and the host tissue (Orive *et al* 2003). We have previously demonstrated the release of neurotrophic and neuroprotective factors from NSCs encapsulated in alginate (Purcell *et al* 2009). Here, we show that combining a cortical prosthesis with this scaffold diminishes the early tissue response and facilitates initial integration of the device with the surrounding brain tissue. Cell seeding is associated with increased neuronal loss and glial encapsulation after 6 weeks. We hypothesize that the evolving response to NSC seeding may be related to changes in cell function and viability over time.

## Materials and methods

### Probe manufacture

The probes were microfabricated in the Lurie Nanofabrication Facility at the University of Michigan using methods previously described, and the process is illustrated in figure 1 (Seymour and Kipke 2007). Briefly, a sacrificial release layer of  $\text{SiO}_2$  was grown on a Si wafer. Parylene-C (Specialty Coating, Indianapolis, IN) was deposited (5  $\mu\text{m}$  thick) via chemical vapor deposition. SU-8 2025 (Microchem, Newton, MA) was spin-coated and patterned to create the core of each tine. Parylene was etched using oxygen plasma RIE. Probes were released using hydrofluoric acid and then thoroughly rinsed in acetone, ethanol and DI water. Final dimensions of the probe were 2.6 mm long, 200  $\mu\text{m}$  wide and 40  $\mu\text{m}$  thick. An opening through the thickness of the device measuring 100  $\mu\text{m}$  across and 2.1 mm in length was designed to carry scaffold material (figures 1, 3(a)). Support arms to this feature had square cross-sections measuring 40  $\mu\text{m}$  on each side.

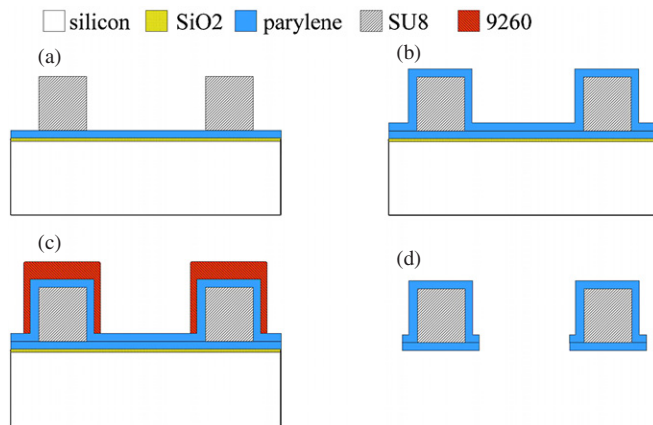


**Figure 1.** Cross-sectional view of wafer level fabrication. (a) Parylene deposited on SiO<sub>2</sub> sacrificial layer and the SU-8 patterned shank. (b) Parylene encapsulated SU-8 structure. (c) 9260 resist patterned to form thick mask over shank. (d) Etched and released final structure. Photolithography masks used steps in (a), (c).

### Cell culture and probe scaffolding

E14 murine cortical NSCs were obtained from StemCell Technologies (Vancouver, BC), cultured as neurospheres and expanded with 20 ng mL<sup>-1</sup> epidermal growth factor (EGF) according to the supplier's protocol. The culture and stem cell characteristics of these cells have been described (Reynolds and Weiss 1992, 1996). The cells are a heterogeneous mixture of stem and progenitor cells (Reynolds and Weiss 1996). Probe scaffolding was achieved by mixing a cell slurry with alginate 50:50, rapidly dip-coating the probe in the mixture, and cross-linking with a 0.1 M calcium chloride solution. The alginate was highly purified with 68% guluronic acid content (MW = 219 000 g/mol) from NovaMatrix (Drammen, Norway). This composition was chosen based on a previous study (Purcell *et al* 2009). Probes had a final concentration of 10 000 000 cells mL<sup>-1</sup> in 1% w/v alginate, resulting in an estimated 100 cells in the microscale probe well based on the well volume. This is an underestimate of the actual number of cells contained on the probe, as the cell-seeded volume appears to coat the surface of the probes as well (figure 3(a)). This additional volume contains approximately 500 cells when the scaffold layer extended an average of 40 μm beyond the probe surface. Non-seeded probes were treated identically to NSC-seeded probes, with the exceptions that cells ('alginate' probes), or both cells and alginate ('probe alone'), were omitted from the coating procedure. Alginate coated probes were prepared by mixing alginate 50:50 with cell culture media. All probes were stored in media prior to implantation.

### Probe implantation

Sixteen male Sprague Dawley rats (300–350 g) were each implanted with four untethered probes (two containing NSC-seeded alginate, one with alginate only, and one untreated probe) using a surgical procedure similar to those previously reported (Vetter *et al* 2004, Seymour and Kipke 2007). Anesthesia was achieved via a ketamine cocktail. A 3 × 3 mm craniotomy was centered over the somatosensory cortex (−2.0 mm AP, ± 4.0 mm ML from Bregma) in each

hemisphere. Dura was resected and two probes (one seeded, one unseeded) were manually inserted in each craniotomy with an approximate 2 mm span between them. Calcium alginate was used for duraplasty followed by surgical closure with silicone and dental acrylic. No immunosuppressive treatments were used. All procedures complied with the United States Department of Agriculture guidelines for the care and use of laboratory animals, and were approved by the University of Michigan Animal Care and Use Committee.

### Histology and quantitative analysis

After implantation, animals were deeply anesthetized and transcardially perfused with 4% paraformaldehyde at the appropriate time point (1 day, 1 week, 6 weeks or 3 months,  $n = 4$  animals per time point). Brain tissue was explanted, postfixed overnight in 4% paraformaldehyde, and cryoembedded following sucrose protection. Probes were left *in situ* for histology. Serial 12 μm thick sections along the shank of the probes were collected, and eight tissue sections between cortical layers II and V were randomly selected and immunostained for NeuN (1:100, Millipore Corporation, Billerica, MA) and Neurofilament (1:1000, Novus Biologicals, Littleton, CO) and counterstained with Hoechst (1 μg mL<sup>-1</sup>, Invitrogen Corporation, Carlsbad, CA) for quantitative analysis of tissue response. Six sections were stained with Ox-42 (1:100, Serotec, Oxford, UK), glial fibrillary acidic protein (GFAP, 1:100), and Hoechst (1 μg mL<sup>-1</sup>) to assess glial encapsulation qualitatively. Six sections per probe were stained for nestin (1:100, StemCell Technologies, Vancouver, BC), GFAP (1:100, Sigma, St Louis, MO), and M2 (1:10, Iowa Hybridoma Bank, Iowa City, IA) for identification of murine-derived NSCs and possible differentiation status. Six additional sections were stained with a neuronal class III β-tubulin (TUJ-1) antibody (1:500, StemCell Technologies, Vancouver, BC), NG-2 (1:500, Millipore Corporation, Billerica, MA) and M2 (1:10, Iowa Hybridoma Bank, Iowa City, IA) to identify neuronal and oligodendrocyte precursors respectively. Six sections per probe were stained for doublecortin (1:1000, Abcam, Cambridge, UK) and M2, and counterstained with Hoechst. Where positive M2 staining was observed, a total of twelve sections were stained with nestin and GFAP and analyzed for a quantification of the expression of these markers as an indication of differentiation status. Approximately 60 cells per animal were counted in the two animals where positive staining was observed.

The immunohistochemistry procedure has been described (Cowell *et al* 2003). Briefly, sections were hydrated in a buffer (PBS or TBS), blocked with 10% normal goat serum, and incubated overnight with primary antibodies at 4 °C. The sections were then rinsed, incubated in the appropriate secondary antibodies (1:200 Alexa-350, 488, and/or 568, Invitrogen), counterstained with Hoechst, and coverslipped with ProLong Gold (Invitrogen). Antibody solutions included 0.3% triton X-100 and 5% normal goat serum. A buffer was used in place of a primary antibody for controls. Confocal images were collected with an Olympus FV500 microscope with a 20× or 40× objective.



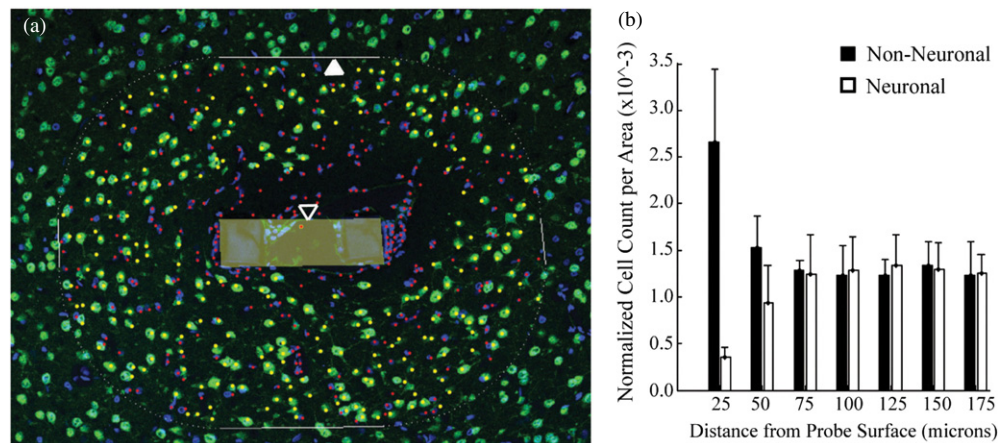


**Figure 2.** Neuronal (NeuN+ in green, Hoechst+ in blue) and non-neuronal (NeuN-, Hoechst+) nuclei counted by a blinded observer (a), and the resulting output (b). The counting boundary (closed arrow) was calculated based on the user-defined probe surface boundary (open arrow, shaded area), and a blinded observer manually selected neuronal and non-neuronal nuclei within this region (shown in yellow and red, respectively). The location of each nucleus relative to the probe surface was counted, binned in 25  $\mu\text{m}$  increments, and normalized to area.

A MatLAB graphical user interface was developed in-house to facilitate cell counting, using a method that has been previously described (Seymour and Kipke 2007). An outline of the exterior edge of the probe cross-section was delineated using a differential interference contrast (DIC) and UV fluorescence image. A blinded technician selected all nuclei as either neuronal (NeuN+, Hoechst+) or non-neuronal (Hoechst+ only) within a software-defined 175  $\mu\text{m}$  radius of the probe surface. A representative image after cell counting and the resulting histograms are illustrated in figure 2. Four optical images (3 mm step size) in each of eight physical sections per probe were analyzed. The software algorithm used the coordinates of the user-selected nuclei to calculate the shortest distance to the probe surface, bin the counts by distance, and calculate the sampling area of each bin to result in neuronal and non-neuronal densities as a function of distance from the probe.

### Statistics

For neuronal and non-neuronal density, eight sections were analyzed for each of four probes per animal, with four animals evaluated for each of four time points. Data were binned into seven 25  $\mu\text{m}$  distance bins from the probe surface; a total of 2688 individual data points for both neuronal and non-neuronal densities were used to generate the statistical models.

A linear mixed effects model was used to evaluate the responses of neuronal density and non-neuronal density due to the clustering of multiple probe evaluations within each animal. The fixed effects were the probe condition, distance, and time. The random effect was the animal subject. Analysis was performed using the statistical package SPSS (Chicago, IL). Results were assessed by Fisher's least significant difference method and termed statistically significant at the  $P = 0.05$  level.

A univariate general linear model was used to assess the correlative relationship between neuronal density and non-neuronal density. Common correlation methods (such as Pearson's correlation) were not used as these techniques do

not take into account the fixed and random effects of the data, and may yield an inflated correlation coefficient. The fixed effects were the probe condition, distance, and time. The random effect was the animal subject. Non-neuronal density was defined as a covariate in order to assess it as a predictor of neuronal density.

## Results and discussion

### Probe design and *in vivo* NSC detection

Parylene devices were successfully designed and fabricated containing a hollow well for scaffold retention (arrow, figures 3(a), (b)). In addition to filling the open channel of the neural probe, a thin layer of scaffold material covered coated probes, and cells were detected slightly outside of the well boundary *in vivo* (figures 3(a), (c), (e)). This exterior scaffold layer varied in size along the shank of each probe, and appeared to be 40  $\mu\text{m}$  thick on average upon visual inspection; probe coatings were similar between devices. Immunohistochemistry for the murine-specific marker M2 allowed for the *in vivo* detection of cortical NSCs derived from embryonic mice based on a previous report (Teng *et al* 2002). Alginate and parylene autofluoresced in green and blue respectively enabling visualization of these structures (figures 3(c)–(e)). NSCs were detected at the 1 day time point *in vivo*, and mainly expressed a combination of nestin and GFAP, with limited doublecortin (DCX, typically indicative of neuronal precursors) expression also observed (figures 3(c)–(e)). Approximately 44% of M2-positive cells were associated with nestin, 5.5% expressed GFAP, and 36% displayed both of these markers, indicating undifferentiated cells, astrocytes, and glial progenitors respectively (Messam *et al* 2000). There was no evidence of M2-positive oligodendrocyte precursors.

The markers observed were similar to those reported in the literature, where the majority of neural stem and progenitor cells express nestin and GFAP, and neuronal and oligodendrocyte markers are observed far less frequently (Reynolds and Weiss 1996, Ourednik *et al* 2002, Teng *et al*

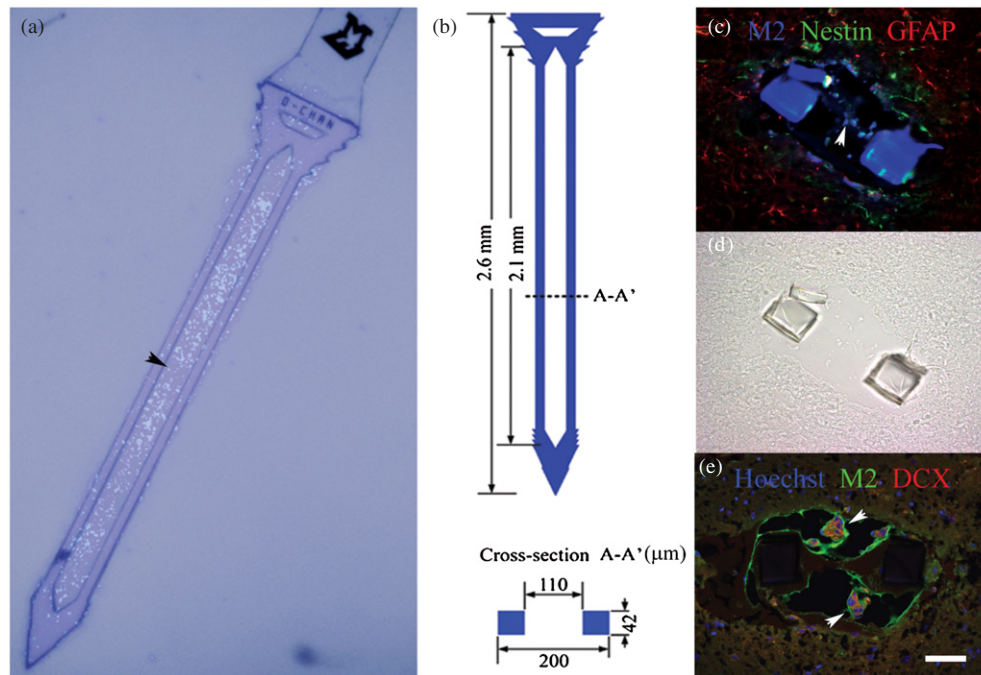


**Figure 3.** A neural stem cell-seeded probe (a), and associated dimensions (b). Cells are Hoechst-stained (a). Cross-section views of neural stem cell-seeded probes 1 day following implantation from two animals (c)–(e). The companion brightfield DIC image for (c) is shown in (d) for reference due to autofluorescence of the parylene probe. Graft cells (M2-labeled) were associated with nestin (c), GFAP (c), and doublecortin (DCX) (e) expression. Scale = 50  $\mu\text{m}$  for (c)–(e).

2002). The somewhat limited detection of NSCs (at the 1 day time point only) and identification of their differentiation status *in vivo* is likely due to the relatively small number of cells initially present in the microscale device and the reportedly large loss (>90%) in progenitor graft cell viability within the initial week following implantation (Sortwell *et al* 2000, Bakshi *et al* 2005). While scaffolds appeared relatively intact 24 h after insertion (figures 3(c), (e)), the loss of graft cells upon insertion is also a possibility.

#### *Scaffold condition effects on neuronal and non-neuronal densities*

Quantitative and qualitative analysis of neuronal and non-neuronal densities within the first 175  $\mu\text{m}$  of the probes revealed the degree of injury around the implants as a function of scaffold condition, time and distance from the probe surface (figures 4–6). NSC-seeded probes had a higher surrounding neuronal density compared to untreated probes at 1 day post-implantation (figure 4(a),  $P = 0.023$ ). Neuronal density was increased around NSC probes compared to both control conditions at the 1 week time point (figure 4(a),  $P \leq 0.002$ ). The experimental probes had reduced non-neuronal encapsulation compared to alginate-only probes at 1 day and untreated probes at 1 week after insertion (figure 4(b);  $P \leq 0.001$ ).

The mitigation of the early tissue response associated with NSC-seeded probes may be due to an initial bystander effect of the cells. The increased neuronal density surrounding seeded probes may result from the secretion of multiple neuroprotective factors by the grafted cells, both known and

yet to be elucidated. We have previously demonstrated the release of brain-derived neurotrophic factor (BDNF), glial-derived neurotrophic factor (GDNF) and nerve growth factor (NGF) from alginate-encapsulated NSCs over a 3 week time period *in vitro* (Purcell *et al* 2009). These neurotrophic factors are known to support neuronal survival and plasticity in various models of axonopathy and neuropathy (Kolb *et al* 1997, Han and Holtzman 2000, Nicole *et al* 2001, Lu *et al* 2003, Wilkins and Compston 2005). The neuroprotective effect of medium conditioned by NSC-seeded alginate beads was further verified using a serum-withdrawal mediated cell death model in PC-12 cells (Purcell *et al* 2009). Alternatively, the increase in neuronal density could be due, in part, to the neuronal differentiation and integration of graft cells into the surrounding brain tissue. However, no direct evidence of this phenomenon was seen in the immunohistochemistry results, and the degree of neuronal density increase is unlikely to be largely explained by the number of cells seeded onto the microscale implant. The production of new neurons by endogenous stem cells originating in the host is an additional, and unexplored, possibility. This also seems improbable as a primary cause of results, as NSCs originating in the subventricular zone have been shown to contribute primarily to astrogliosis, with neuronal differentiation rarely observed following migration to the site of cortical trauma (Salman *et al* 2004). However, it is worth noting that evidence of doublecortin positivity was observed in one graft (figure 3(e)), as well as in host tissue 1 week after implantation (supplementary figure 1, available at [stacks.iop.org/JNE/6/026005](http://stacks.iop.org/JNE/6/026005)). Doublecortin (DCX) is a microtubule-associated protein expressed primarily

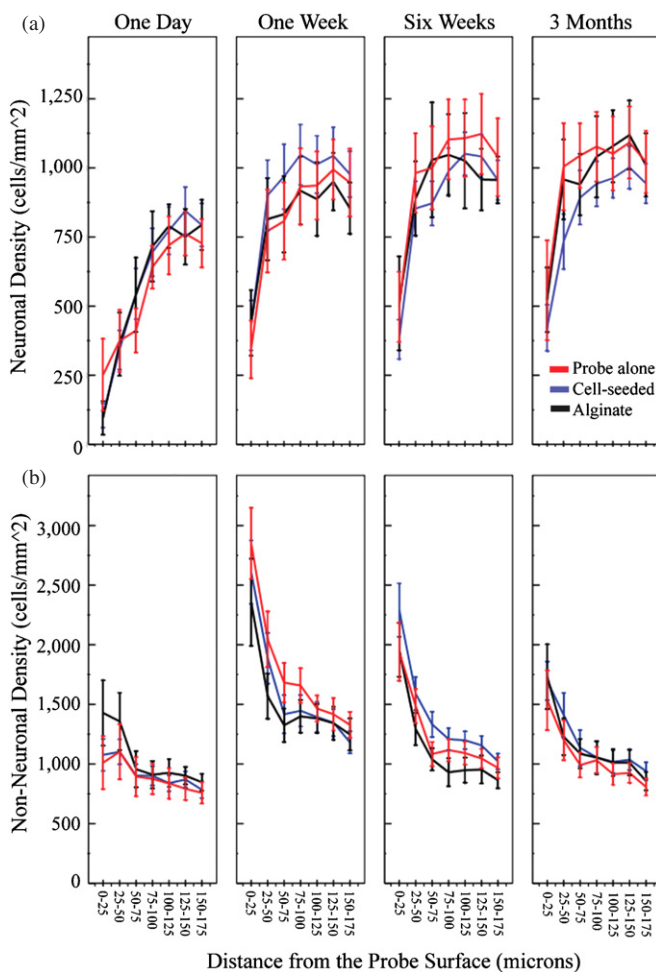


**Figure 4.** Mean neuronal density (a) and non-neuronal density (b) surrounding implants over time as a function of distance from the probe surface ( $\pm$ s.e.m). NSC-seeded probes had a higher neuronal density surrounding them compared to untreated probes at 1 day and both control conditions at 1 week post-implant (a),  $P < 0.05$ . Cell seeding reduced non-neuronal encapsulation compared to alginate-only probes at 1 day and untreated probes at 1 week post-implant ( $P \leq 0.001$ ). At 6 weeks and 3 months post-implantation, the NSC-seeded probes had reduced neuronal density and increased non-neuronal density surrounding them in comparison to both control conditions ( $P < 0.05$ ).

in migrating neuronal precursors, and reportedly may also be associated with mature astrocytes according to Verwer *et al* (Francis *et al* 1999, Verwer *et al* 2007). Expression of DCX around neural implants has not been previously reported in the literature, and may represent an additional target for future strategies to improve device-tissue integration if its presence indicates a regenerative capacity of the injured brain, the grafted cells, or a combination of both.

At 6 weeks and 3 months post-implantation, the NSC-seeded probes had reduced neuronal density and increased non-neuronal encapsulation surrounding them in comparison to both control conditions (figures 4(a), (b),  $P \leq 0.049$  for neuronal density at 6 weeks,  $P \leq 0.001$  at 3 months,  $P < 0.001$  for non-neuronal density at both time points). This effect may be due to reduced NSC viability over time, which has been reported previously and may be aggravated by degradation of

the alginate scaffold (Sortwell *et al* 2000, Bakshi *et al* 2005). Alginate stability drops markedly during the first 24 h *in vivo*, and is prone to fragmentation over the following 3 months (Nunamaker *et al* 2007). This may leave the grafted cells vulnerable to an immune reaction, and such a response could account for the exacerbation of the tissue response after 6 weeks. We hypothesize that reduced graft cell viability and function over time, followed by a secondary inflammatory reaction to cellular debris, may explain the deleterious effect of cell seeding at later time points. It is also possible that an early reduction of glial activation by NSCs intensifies neuronal injury later (Hanisch and Kettenmann 2007). However, elucidating the mechanism behind the effects of NSC seeding is left as the subject of future studies that more directly assess graft cell viability and function over time.

Alginate coating (without cell seeding) had no effect on neuronal density surrounding probes over the course of the study (figure 4(a)). However, alginate coating yielded mixed effects on non-neuronal density (figure 4(b)). The evolving tissue response to alginate probes may be related to the degradation of the hydrogel over time. We have published a previous report in which alginate disks with various compositions were implanted subcutaneously in rats and assessed over time for mechanical stability and biocompatibility. The results indicated an initial collapse of all alginate samples within the first 24 h of implantation, as evidenced by a dramatic 80% drop in the complex modulus. This metric was stable for the following 3 weeks (Nunamaker *et al* 2007). One day after implantation, alginate coated probes in the present study had a significantly higher non-neuronal density than NSC-seeded and control probes (figure 4(b),  $P \leq 0.001$ ). This effect was especially pronounced within the first 50  $\mu$ m of the probe surface. An initial loss of calcium ions and/or water to the surrounding tissue, causing a potentially injurious, non-isotonic environment resulting in glial activation, could explain this. Interestingly, cell-seeded alginate does not exhibit this initial activation of glia; the encapsulated cells may buffer the surrounding tissue from this effect (figure 5). One week after implantation, alginate probes reduce non-neuronal density in comparison to untreated probes, likely due to the non-adhesive nature of the gel ( $P < 0.001$ ) (Rowley *et al* 1999). Alternatively, alginate may buffer the mechanical mismatch between the probe and surrounding brain tissue, and reduce glial encapsulation as a consequence. Alginate was stable during the first week *in vivo* according to histological evaluation in our previous report, after which it progressively fragmented, appearing to be largely infiltrated by tissue in-growth 3 months after implantation (Nunamaker *et al* 2007). By 6 weeks post-implantation, alginate and untreated probes have equivalent non-neuronal densities surrounding them. The alginate is likely to have significantly degraded by this point.

#### *Neuronal and non-neuronal densities as a function of distance*

Neuronal density increased as a function of distance from the probe, and non-neuronal density decreased reciprocally.



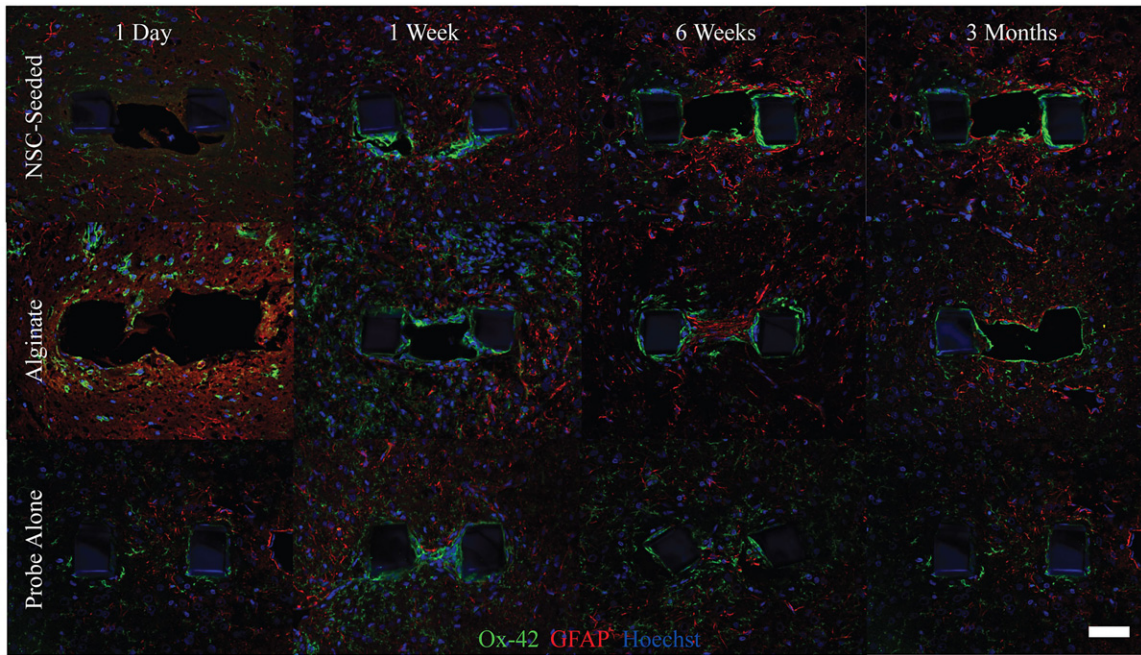


**Figure 5.** Glial encapsulation of each probe condition over the 3 month time course. Ox-42 labeled microglia and GFAP labeled astrocytes are shown. Images are taken from probes implanted in the same animal at each time point. NSC seeding was associated with reduced non-neuronal density at 1 day post-implantation in comparison to alginate coated probes and at the 1 week time point in comparison to untreated probes ( $P < 0.001$ ). Glial activation is at its overall peak 1 week after insertion. A thin encapsulation layer surrounds probes at the 6 week and 3 month time points, with NSC-seeded probes having the greatest surrounding non-neuronal density ( $P < 0.001$ ). Interestingly, microglia appeared to have a ramified, or ‘surveilling’, morphology surrounding a neural stem cell-alginate probe initially, whereas activated cells with an amoeboid structure were found near an alginate probe in the same hemisphere of one animal (left panels).

Neuronal density was minimal in the first  $25 \mu\text{m}$  of the probe, with significant incremental increases in the  $25\text{--}50$ ,  $50\text{--}75$ , and  $75\text{--}100 \mu\text{m}$  bins (figure 4(a),  $P < 0.001$ ). Neuronal density stabilized thereafter. The loss of neuronal soma within the first  $100 \mu\text{m}$  of the probe is particularly concerning, considering that reliably sorted, large amplitude spikes are recorded when neurons are within  $50 \mu\text{m}$  of recording sites, and no discernable signals are detected from cells greater than  $140 \mu\text{m}$  from probes (Henze *et al* 2000). There was a significant decrease in non-neuronal density as a function of distance from the probe surface (figure 4(b)). Non-neuronal density was highest in the  $0\text{--}25 \mu\text{m}$  bin, and significantly decreased in the  $25\text{--}50 \mu\text{m}$  bin, followed by a further decrease in the  $50\text{--}75 \mu\text{m}$  bin ( $P < 0.001$ ). Non-neuronal density stabilized thereafter ( $P = 0.001$ ). Again, the greatest glial encapsulation of the device occurred in the region yielding the highest quality signals. The observation that the tissue response is the most severe in the recordable region surrounding the probe indicates that this phenomenon may result in recording instability, and corroborates previous reports (Szarowski *et al* 2003, Kim *et al* 2004, Biran *et al* 2005).

#### *The correlation between neuronal and non-neuronal densities*

There was a significant negative correlation between neuronal and non-neuronal densities (figures 4(a), (b),  $P < 0.001$ ). This result expands upon previous work, which has demonstrated an inverse relationship between microglial and neurofilament

staining as a function of distance from implanted probes (Biran *et al* 2005). Possible reasons for this relationship include physical displacement of neurons by glia and deleterious effects on neuronal viability and axonal outgrowth by the glial scar. Our results indicate the latter, as clustering of displaced neurons was not observed in the density data. Further, reactive microglia involved in the injury response to probes are known to elute potentially neurotoxic inflammatory cytokines, and reactive astrocytes may produce proteoglycans inhibitory to axonal regeneration (Silver and Miller 2004, Biran *et al* 2005).

#### *Neuronal and non-neuronal densities as a function of time*

There are general trends in the distribution of neurons and non-neurons surrounding the devices as a function of time. Neurofilament disruption indicative of axonal damage was evident immediately after implantation for all conditions and accompanied the dramatic loss of neuronal density within the first  $100 \mu\text{m}$  of the probe surface (figures 6 and 4(a),  $P \leq 0.036$ ) (Chen *et al* 1999). This injury response appeared considerably improved 1 week after surgery, and neuronal density was significantly increased at this time (figures 6 and 4(a),  $P < 0.01$ ). Values stabilized thereafter. Non-neuronal density is lowest 1 day after transplantation, followed by a peak value of this metric 1 week after implantation (figures 5 and 4(b),  $P < 0.05$ ). By 6 weeks, a thin glial sheath surrounded all probes, with non-neuronal densities progressively decreasing through the 3 month time point (figures 5 and 4(b),  $P <$

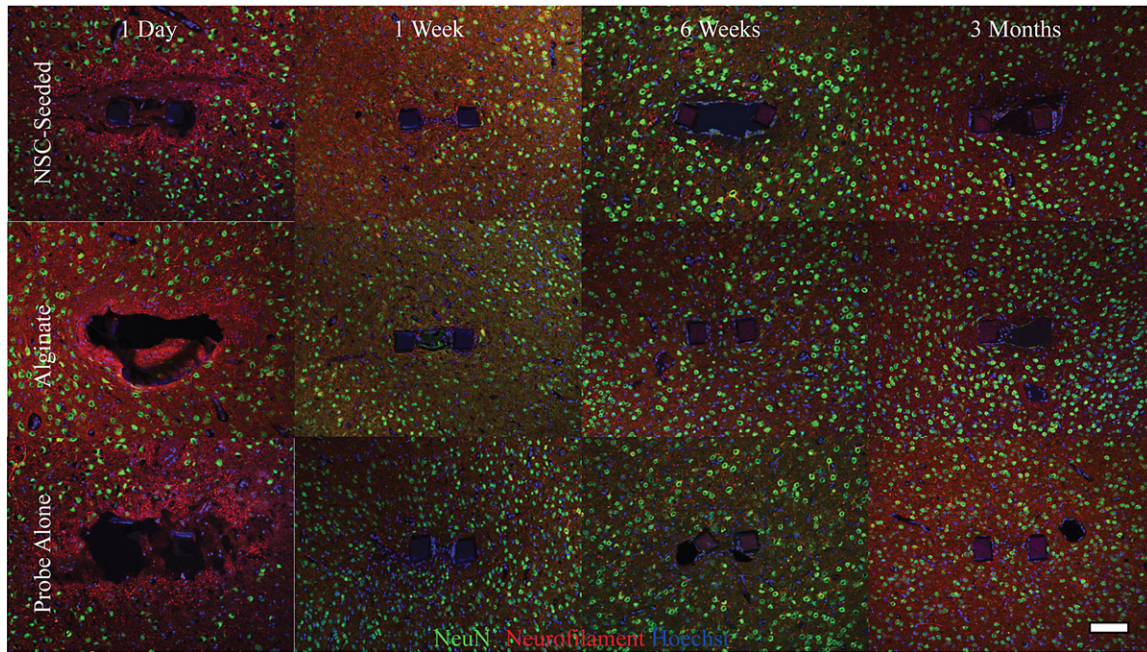


**Figure 6.** Immunohistochemistry for neuronal markers (NeuN and neurofilament) reveals an initial injury response in which neuronal soma are distanced from the probe, and neurofilament disruption indicative of damaged axons is seen 1 day after implantation. A marked improvement in the appearance of the injury site occurs within the first week, with a significant increase in neuronal density surrounding probes evident at this time point ( $P \leq 0.006$ ). NSC seeding was associated with the increased neuronal density surrounding prostheses in the first week of implantation, with a reversal of this effect at later time points ( $P < 0.05$ ).

0.001). These results corroborate a qualitative study of the glial encapsulation of silicon probes (Szarowski *et al* 2003). Sustained glial activation and neuronal density loss within the first 100  $\mu\text{m}$  surrounding the insertion site of silicon probes was reported in a study which quantified these responses after 2 and 4 weeks *in vivo* (Biran *et al* 2005). In these studies, the use of silicon probes necessitated the removal of the devices prior to tissue processing, potentially disrupting the interface. Our results are in general agreement with these reports in the literature, and expand upon them as a quantitative dataset studying an intact device–tissue interface over multiple time points spanning 3 months.

Changes in neuronal density surrounding neural prostheses as a function of time have not been demonstrated previously in the literature, and the relationship between recording performance and neuronal density remains unknown. It should be noted that the devices in this study have inherently different geometries and material properties than those typically examined in the literature, potentially altering their interaction with the brain. Nonetheless, it is interesting to compare the time course of neuronal density changes observed in this study to the degradation of recording performance typically reported for microwires and silicon-based devices. The initially severe injury seen following insertion, followed by a return of neuronal soma near the probe at 1 week, corresponds well with the variation in recording quality observed with silicon probes; there is typically a loss and recovery of unit recordings generally corresponding to this time course (Ludwig *et al* 2006). However, recording quality often diminishes over subsequent weeks and months, and this is not predicted by the general improvements in 6

week and 3 month neuronal and non-neuronal density data. It may be that any improvement in recorded signal derived from increased neuronal density is negated by the compact glial sheath formed at later time points. Astrogliosis is known to impede ionic transfer through tissue (Roitbak and Sykova 1999). Alternatively, the data raise the possibility of neuronal plasticity and the formation of silent synapses as additional explanations for recording instability. Henze *et al* have reported detecting approximately six units per tetrode, despite estimations that 60–100 neurons should have sufficient amplitude to be discernible above noise (Henze *et al* 2000). Whether or not the neurons located within a recordable distance from electrodes are functionally normal or not is unknown. Understanding not only changes in the structure, but also the function, of tissue surrounding the probes may enable additional intervention strategies to improve recording stability.

## Conclusions

We developed a novel, cell-seeded cortical neural prosthesis and evaluated its histological effects *in vivo*. Our data show that NSC seeding was related to an attenuation of the initial tissue response associated with the introduction of a foreign body into the brain. Given the physical isolation of the graft cells from the surrounding tissue, *in vitro* data demonstrating the secretion of neuroprotective factors by the scaffold (Purcell *et al* 2009), and current evidence that the majority of cells express nestin initially *in vivo*, a bystander effect may be responsible. Doublecortin-positive immature neurons were associated primarily with seeded probes 1 week



after implantation, possibly indicating a regenerative capacity of the injured brain, graft cells, or both. Degradation of the alginate scaffold may leave transplanted cells vulnerable to immune rejection at later time points. An inflammatory reaction to cellular debris could explain the detrimental effect of cell seeding by 6 weeks post-implant. Future studies of this biohybrid device will include investigating these mechanisms further and functionalizing recording sites for neurophysiology studies.

## Acknowledgments

The authors gratefully thank Aparna Singh for surgical assistance and Joe Kazemi from the Center for Statistical Consultation and Research at the University of Michigan for guidance with the mixed model development. The M2 antibody was obtained from the Developmental Studies Hybridoma Bank, where it was developed under the auspices of the NICHD and maintained by The University of Iowa, Department of Biological Sciences, Iowa City, IA 52242. This work was supported by the Center for Neural Communication Technology (NIBIB, P41-EB002030).

## References

- Bakshi A *et al* 2005 Caspase-mediated cell death predominates following engraftment of neural progenitor cells into traumatically injured rat brain *Brain Res.* **1065** 8–19
- Biran R *et al* 2005 Neuronal cell loss accompanies the brain tissue response to chronically implanted silicon microelectrode arrays *Exp. Neurol.* **195** 115–26
- Carmena J M *et al* 2003 Learning to control a brain–machine interface for reaching and grasping by primates *PLoS Biol.* **1** E42
- Chen X H *et al* 1999 Evolution of neurofilament subtype accumulation in axons following diffuse brain injury in the pig *J. Neuropathol. Exp. Neurol.* **58** 588–96
- Cowell R M *et al* 2003 Complement activation contributes to hypoxic-ischemic brain injury in neonatal rats *J. Neurosci.* **23** 9459–68
- Donoghue J P *et al* 2007 Assistive technology and robotic control using motor cortex ensemble-based neural interface systems in humans with tetraplegia *J. Physiol.* **579** Pt 3 603–11
- Edell D J *et al* 1992 Factors influencing the biocompatibility of insertable silicon microshafts in cerebral cortex *IEEE Trans. Biomed. Eng.* **39** 635–43
- Fitzsimmons N A *et al* 2007 Primate reaching cued by multichannel spatiotemporal cortical microstimulation *J. Neurosci.* **27** 5593–602
- Francis F *et al* 1999 Doublecortin is a developmentally regulated, microtubule-associated protein expressed in migrating and differentiating neurons *Neuron* **23** 247–56
- Gaillard A *et al* 2007 Reestablishment of damaged adult motor pathways by grafted embryonic cortical neurons *Nat. Neurosci.* **10** 1294–9
- Han B H and Holtzman D M 2000 BDNF protects the neonatal brain from hypoxic-ischemic injury *in vivo* via the ERK pathway *J. Neurosci.* **20** 5775–81
- Hanisch U K and Kettenmann H 2007 Microglia: active sensor and versatile effector cells in the normal and pathologic brain *Nat. Neurosci.* **10** 1387–94
- Heine W *et al* 2004 Transplanted neural stem cells promote axonal regeneration through chronically denervated peripheral nerves *Exp. Neurol.* **189** 231–40
- Henze D A *et al* 2000 Intracellular features predicted by extracellular recordings in the hippocampus *in vivo* *J. Neurophysiol.* **84** 390–400
- Hochberg L R *et al* 2006 Neuronal ensemble control of prosthetic devices by a human with tetraplegia *Nature* **442** 164–71
- Itoh T *et al* 2007 Immature and mature neurons coexist among glial scars after rat traumatic brain injury *Neurol. Res.* **29** 734–42
- Kennedy P R 1989 The cone electrode: a long-term electrode that records from neurites grown onto its recording surface *J. Neurosci. Methods* **29** 181–93
- Kennedy P R *et al* 1992 The cone electrode: ultrastructural studies following long-term recording in rat and monkey cortex *Neurosci. Lett.* **142** 89–94
- Kim Y T *et al* 2004 Chronic response of adult rat brain tissue to implants anchored to the skull *Biomaterials* **25** 2229–37
- Klueh U *et al* 2005 Enhancement of implantable glucose sensor function *in vivo* using gene transfer-induced neovascularization *Biomaterials* **26** 1155–63
- Kolb B *et al* 1997 Nerve growth factor stimulates growth of cortical pyramidal neurons in young adult rats *Brain Res.* **751** 289–94
- Lebedev M A and Nicolelis M A 2006 Brain–machine interfaces: past, present and future *Trends Neurosci.* **29** 536–46
- Lindvall O *et al* 2004 Stem cell therapy for human neurodegenerative disorders—how to make it work *Nat. Med.* **10** Suppl S42–50
- Liu X *et al* 1999 Stability of the interface between neural tissue and chronically implanted intracortical microelectrodes *IEEE Trans. Rehabil. Eng.* **7** 315–26
- Liu X *et al* 2006 Evaluation of the stability of intracortical microelectrode arrays *IEEE Trans. Neural Syst. Rehabil. Eng.* **14** 91–100
- Llado J *et al* 2004 Neural stem cells protect against glutamate-induced excitotoxicity and promote survival of injured motor neurons through the secretion of neurotrophic factors *Mol. Cell. Neurosci.* **27** 322–31
- Lu P *et al* 2003 Neural stem cells constitutively secrete neurotrophic factors and promote extensive host axonal growth after spinal cord injury *Exp. Neurol.* **181** 115–29
- Ludwig K A *et al* 2006 Chronic neural recordings using silicon microelectrode arrays electrochemically deposited with a poly(3,4-ethylenedioxythiophene) (PEDOT) film *J. Neural Eng.* **3** 59–70
- Messam C A *et al* 2000 Coexpression of nestin in neural and glial cells in the developing human CNS defined by a human-specific anti-nestin antibody *Exp. Neurol.* **161** 585–96
- Nicole O *et al* 2001 Neuroprotection mediated by glial cell line-derived neurotrophic factor: involvement of a reduction of NMDA-induced calcium influx by the mitogen-activated protein kinase pathway *J. Neurosci.* **21** 3024–33
- Nicolelis M A *et al* 2003 Chronic, multisite, multielectrode recordings in macaque monkeys *Proc. Natl. Acad. Sci. USA* **100** 11041–6
- Nunamaker E A *et al* 2007 *In vivo* stability and biocompatibility of implanted calcium alginate disks *J. Biomed. Mater. Res. A* **83** 1128–37
- Orive G *et al* 2003 Cell encapsulation: promise and progress *Nat. Med.* **9** 104–7
- Ourednik J *et al* 2002 Neural stem cells display an inherent mechanism for rescuing dysfunctional neurons *Nat. Biotechnol.* **20** 1103–10
- Pluchino S *et al* 2005 Neurosphere-derived multipotent precursors promote neuroprotection by an immunomodulatory mechanism *Nature* **436** 266–71
- Polikov V S *et al* 2005 Response of brain tissue to chronically implanted neural electrodes *J. Neurosci. Methods* **148** 1–18
- Prichard H L *et al* 2007 Adult adipose-derived stem cell attachment to biomaterials *Biomaterials* **28** 936–46

- Prichard H L *et al* 2008 IFATS collection: adipose-derived stromal cells improve the foreign body response *Stem Cells* **26** 2691–95
- Purcell E K *et al* 2009 *In vitro* development and characterization of a cortical neural stem cell-seeded alginate scaffold *Tissue Eng. C* at press
- Rejali D *et al* 2007 Cochlear implants and *ex vivo* BDNF gene therapy protect spiral ganglion neurons *Hear. Res.* **228** 180–7
- Reynolds B A and Weiss S 1992 Generation of neurons and astrocytes from isolated cells of the adult mammalian central nervous system *Science* **255** 1707–10
- Reynolds B A and Weiss S 1996 Clonal and population analyses demonstrate that an EGF-responsive mammalian embryonic CNS precursor is a stem cell *Dev. Biol.* **175** 1–13
- Roitbak T and Sykova E 1999 Diffusion barriers evoked in the rat cortex by reactive astrogliosis *Glia* **28** 40–8
- Rousche P J and Normann R A 1998 Chronic recording capability of the Utah intracortical electrode array in cat sensory cortex *J. Neurosci. Methods* **82** 1–15
- Rowley J A *et al* 1999 Alginate hydrogels as synthetic extracellular matrix materials *Biomaterials* **20** 45–53
- Salman H *et al* 2004 Subventricular zone neural stem cells remodel the brain following traumatic injury in adult mice *J. Neurotrauma* **21** 283–92
- Schwartz A B *et al* 2006 Brain-controlled interfaces: movement restoration with neural prosthetics *Neuron* **52** 205–20
- Seymour J P and Kipke D R 2007 Neural probe design for reduced tissue encapsulation in CNS *Biomaterials* **28** 3594–607
- Silver J and Miller J H 2004 Regeneration beyond the glial scar *Nat. Rev. Neurosci.* **5** 146–56
- Sortwell C E *et al* 2000 Time course of apoptotic cell death within mesencephalic cell suspension grafts: implications for improving grafted dopamine neuron survival *Exp. Neurol.* **165** 268–77
- Stieglitz T *et al* 2002 A biohybrid system to interface peripheral nerves after traumatic lesions: design of a high channel sieve electrode *Biosens. Bioelec.* **17** 685–96
- Stieglitz T 2007 Restoration of neurological functions by neuroprosthetic technologies: future prospects and trends towards micro-, nano-, and biohybrid systems *Acta Neurochir. Suppl.* **97** Pt 1 435–42
- Szarowski D H *et al* 2003 Brain responses to micro-machined silicon devices *Brain Res.* **983** 23–35
- Taylor D M *et al* 2002 Direct cortical control of 3D neuroprosthetic devices *Science* **296** 1829–32
- Teng Y D *et al* 2002 Functional recovery following traumatic spinal cord injury mediated by a unique polymer scaffold seeded with neural stem cells *Proc. Natl. Acad. Sci. USA* **99** 3024–9
- Turner J N *et al* 1999 Cerebral astrocyte response to micromachined silicon implants *Exp. Neurol.* **156** 33–49
- Velliste M *et al* 2008 Cortical control of a prosthetic arm for self-feeding *Nature* **453** 1098–101
- Verwer R W *et al* 2007 Mature astrocytes in the adult human neocortex express the early neuronal marker doublecortin *Brain* **130** Pt 12 3321–35
- Vetter R J *et al* 2004 Chronic neural recording using silicon-substrate microelectrode arrays implanted in cerebral cortex *IEEE Trans. Biomed. Eng.* **51** 896–904
- Wilkins A and Compston A 2005 Trophic factors attenuate nitric oxide mediated neuronal and axonal injury *in vitro*: roles and interactions of mitogen-activated protein kinase signalling pathways *J. Neurochem.* **92** 1487–96
- Williams J C *et al* 1999 Long-term neural recording characteristics of wire microelectrode arrays implanted in cerebral cortex *Brain Res. Brain Res. Protoc.* **4** 303–13
- Williams J C *et al* 2007 Complex impedance spectroscopy for monitoring tissue responses to inserted neural implants *J. Neural. Eng.* **4** 410–23